THE JOURNAL OF BIOLOGICAL CHEMISTRY VOL. 288, NO. 40, pp. 28514–28523, October 4, 2013

The Mechanism of the Amidases

MUTATING THE GLUTAMATE ADJACENT TO THE CATALYTIC TRIAD INACTIVATES THE ENZYME DUE TO SUBSTRATE MISPOSITIONING[*][S]

Received for publication, July 18, 2013 Published, JBC Papers in Press, August 14, 2013, DOI 10.1074/jbc.M113.503284

Brandon W. Weber[‡], Serah W. Kimani[‡§], Arvind Varsani[‡¶‖], Donald A. Cowan[‡‡], Roger Hunter[§§], Gerhard A. Venter[§§], James C. Gumbart[¶¶1], and B. Trevor Sewell[‡‖‖2]**

From the [‡]Structural Biology Research Unit, Division of Medical Biochemistry, Department of Clinical Laboratory Sciences and [‖‖]Institute of Infectious Diseases and Molecular Medicine, University of Cape Town, Observatory, Western Cape 7925, South Africa, [§]Department of Molecular and Cell Biology, University of Cape Town, University Avenue, Rondebosch, Western Cape 7700, South Africa, [¶]School of Biological Sciences and [‖]Biomolecular Interaction Centre, University of Canterbury, Private Bag 4800, Christchurch 8140, New Zealand, [**]Institute for Microbial Biotechnology and Metagenomics, Department of Biotechnology, University of the Western Cape, Bellville 7535, Cape Town, South Africa, [‡‡]Department of Genetics, University of Pretoria, Pretoria 0002, South Africa, [§§]Scientific Computing Research Unit, Department of Chemistry, University of Cape Town, Rondebosch 7700, South Africa, and [¶¶]School of Physics, Georgia Institute of Technology, Atlanta, Georgia 30332

Background: A cysteine, a glutamic acid, and a lysine are the well known amidase catalytic residues.
Results: Mutating the neighboring, structurally conserved Glu-142 inactivates the enzyme, but the active site cysteine still reacts with acrylamide via its double bond.
Conclusion: Glu-142 positions the amide for productive nucleophilic attack by the cysteine.
Significance: An intact catalytic tetrad is required for amidase activity.

All known nitrilase superfamily amidase and carbamoylase structures have an additional glutamate that is hydrogen bonded to the catalytic lysine in addition to the Glu, Lys, Cys "catalytic triad." In the amidase from *Geobacillus pallidus*, mutating this glutamate (Glu-142) to a leucine or aspartate renders the enzyme inactive. X-ray crystal structure determination shows that the structural integrity of the enzyme is maintained despite the mutation with the catalytic cysteine (Cys-166), lysine (Lys-134), and glutamate (Glu-59) in positions similar to those of the wild-type enzyme. In the case of the E142L mutant, a chloride ion is located in the position occupied by Glu-142 $O^{\epsilon 1}$ in the wild-type enzyme and interacts with the active site lysine. In the case of the E142D mutant, this site is occupied by Asp-142 $O^{\delta 1}$. In neither case is an atom located at the position of Glu-142 $O^{\epsilon 2}$ in the wild-type enzyme. The active site cysteine of the E142L mutant was found to form a Michael adduct with acrylamide, which is a substrate of the wild-type enzyme, due to an interaction that places the double bond of the acrylamide rather than the amide carbonyl carbon adjacent to the active site cysteine. Our results demonstrate that in the wild-type active site a crucial role is played by the hydrogen bond between Glu-142 $O^{\epsilon 2}$ and the substrate amino group in positioning the substrate with the correct stereoelectronic alignment to enable the nucleophilic attack on the carbonyl carbon by the catalytic cysteine.

Amidases of the nitrilase superfamily, which catalyze the hydrolysis of an amide, leading to the formation of carboxylic acid and ammonia, play a role in important metabolic processes. For example, hNit2/ω-amidase catalyzes the hydrolysis of α-ketoglutaramate (the α-keto analog of glutamine) and α-ketosuccinamate (the α-keto analog of asparagine), yielding α-ketoglutarate and oxaloacetate, respectively (1, 2). Sequence homology within the nitrilase superfamily identifies the catalytic triad, which in the amidase from *Geobacillus pallidus* corresponds to Cys-166, Glu-59, and Lys-134 (3, 4). A second structurally conserved glutamate (equivalent to Glu-142) is not recognizable from sequence conservation alone as it is located in a loop of variable length on an exposed surface of the enzyme. The catalytic role of the second glutamate has never been elucidated in detail, but it has been shown to be essential for catalysis in the case of the formamidase from *Bacillus cereus* CECT 5050T (5). It has therefore been postulated that the catalytic mechanism of the amidases require four essential amino acid side chains in a precisely conserved geometry (5–8): a cysteine (Cys-166), two glutamates (Glu-59 and Glu-142), and a lysine (Lys-134).

The amidase reaction proceeds via a ping-pong bi-bi mechanism involving binding of the amide substrate, the release of ammonia, the formation of a thioester intermediate at the cysteine, the binding of water as the second substrate, and finally the release of the carboxylic acid product (9–11). The first crystal structure of a member of the superfamily, a carbamoylase from *Agrobacterium* sp. strain KNK712, led to the proposal that the glutamate (equivalent to Glu-59) enhances the nucleophilicity of the cysteine enabling it to attack the carbonyl carbon of the amide. The proposal that the glutamate at this location enhances the nucleophilicity of the cysteine has found wide acceptance in the nitrilase and amidase literature (9, 12–14).

* This work was supported by grants from the National Research Foundation and the Carnegie Corporation of New York.
[S] This article contains a supplemental video.
The atomic coordinates and structure factors (codes 4kzf, 4lf0, 4gyn, and 4gyl) have been deposited in the Protein Data Bank (http://wwpdb.org/).
[1] Supported by Grant K22-AI100927 from the National Institutes of Health.
[2] To whom correspondence should be addressed: Structural Biology Research Unit, Dept. of Clinical Laboratory Sciences, Inst. of Infectious Diseases and Molecular Medicine, University of Cape Town, Observatory, Western Cape 7925, South Africa. Tel.: 2721-650-2817; Fax: 2721-689-1528; E-mail: Trevor.Sewell@uct.ac.za.

The crystal structures of four amidases are known at resolutions below 2 Å. Three are very similar hexamers (Protein Data Bank codes 2plq (6), 2uxy (15), and 2dyu (9), whereas the fourth is a dimer (7) (Protein Data Bank code 3hkx). The structure of the amidase from *Pseudomonas aeruginosa* (Protein Data Bank code 2uxy) (15) serendipitously visualizes the tetrahedral intermediate, which is formed following the nucleophilic attack by hydroxylamine on the thioester intermediate and thus provides useful mechanistic insights. The structure suggests that (*a*) the pK_a of the lysine is increased by its interaction with the two active site glutamates (Glu-59 and Glu-142), ensuring that it remains protonated; (*b*) hydrogen bonds between the substrate carbonyl oxygen and both the lysine and the backbone amide of the residue next in sequence after the cysteine promote the initial attack of the cysteine on the substrate carbonyl carbon; and (*c*) these same interactions stabilize the oxyanion formed on the oxygen of the hydroxamic group of the tetrahedral intermediate (15).

Different roles of the second glutamate (equivalent to Glu-142) have been suggested during the studies of amidases and D-amino acid carbamoylases. Hung *et al.* (9) noted the role of the residue in the formamidase (AmiF) from *Helicobacter pylori* in maintaining the geometry of the active site and in facilitating the docking of the substrate into the active site. The carbamoylase structures from *Agrobacterium radiobacter* (16) and those deposited by Hashimoto *et al.* (Protein Data Bank codes 1uf4, 1uf5, 1uf7, and 1uf8)[3] in which a substrate is visualized in complex with an inactive enzyme having the active site cysteine substituted by an alanine show the amino group of the substrate hydrogen bonded to an oxygen, $O^{\epsilon 2}$, of the Glu-142 carboxylate. A comparable hydrogen bonding arrangement was seen in the C166S mutant of the formamidase from *H. pylori* that contained a bound formamide (9). The other carboxylate oxygen, $O^{\epsilon 1}$, of Glu-142 is hydrogen bonded to the ζ-amino group of the active site lysine in most known structures of members of the nitrilase superfamily. Kimani *et al.* (6) suggested a catalytic role for the residue in which it acts as a general base catalyst for the hydrolysis of the thioester intermediate. A role for the glutamate equivalent to Glu-142 in the catalysis was confirmed in the case of the formamidase of *B. cereus* CECT (5) by the creation of an inactive mutant in which this residue was replaced by an aspartate. The mutant enzyme was verified to be folded by circular dichroism, but the experiments were unable to distinguish whether the loss of activity was due to failure of the aspartate to polarize the lysine of the catalytic triad or whether it failed to act as a general base catalyst.

In this study, we probed the role of Glu-142 by substituting the residue in the amidase from *G. pallidus* RAPc8 with either a leucine (E142L) or an aspartate (E142D). No activity was observed in either case with any substrate. A possible consequence of this substitution, consistent with the hypothesis of Kimani *et al.* (6), is that the substrate will react with the cysteine forming the thioester but will not be hydrolyzed; this would constitute evidence that the residue is acting as a general base catalyst. Although no such reaction was observed, an alternative outcome was seen in the case of the E142L mutant and the acrylamide substrate: a Michael adduct was formed with the cysteine. Based on the results summarized above, this suggests that the inactivity of the mutant is due to mispositioning of the substrate, thus inhibiting the nucleophilic attack of the cysteine.

[3] H. Hashimoto, M. Aoki, T. Shimizu, T. Nakai, H. Morikawa, Y. Ikenaka, S. Takahashi, and M. Sato, unpublished data.

EXPERIMENTAL PROCEDURES

Synthesis of E142L and E142D Mutants—The plasmid used for the expression of the wild-type amidase from *G. pallidus* RAPc8 (NRRL B-59396) was prepared as described by Cameron *et al.* (21). The glutamate at residue 142 was mutated to a leucine or aspartic acid by simple site-directed mutagenesis. The mutagenesis was carried out using pairs of overlapping primers (E142D, 5′-CCT TGG TGT CCG ATC CTC GGA TGG TAT CC-3′/5′-GGA TAC CAT CCG AGG ATC GGA CAC CAA GG-3′; E142L, 5′-CCT TGG TGT CCG ATC GAT GGA TGG TAT CC-3′/5′-GGA TAC CAT CCA TCG ATC GGA CAC CAA GG-3′) with Accuzyme DNA polymerase (Biolione), which has 3′ → 5′ proofreading activity. On completion, the mutagenesis PCR was digested with DpnI restriction enzyme to fragment the methylated template plasmid DNA. E. cloni (Lucigen) competent cells were transformed with 2 μl of the digested PCR product, and the resulting colonies were screened for the mutation by sequencing (Macrogen Inc., Korea). The mutated construct was transformed into *E. coli* BL21 cells (Lucigen) for expression.

Expression and Purification of the E142L and E142D Mutant Amidases—The protein was expressed and purified according to the method of Agarkar *et al.* (22) with slight modifications. Briefly, *E. coli* BL21 cells harboring the plasmid were grown to logarithmic growth stage in nutrient broth and induced with 1 mM isopropyl 1-thio-β-D-galactopyranoside (Roche Applied Science) for 3 h at 37 °C. Cells were then pelleted at 4000 × *g* for 20 min at 4 °C and stored at −20 °C overnight. The frozen pellet was thawed on ice and resuspended in 20 mM potassium phosphate buffer, pH 7.4 containing 5 mM dithiothreitol (DTT) and protease inhibitor mixture (Roche Applied Science). Sonication was performed on ice using a Misonix 3000 sonicator, and the lysate was centrifuged at 20,000 × *g* for 30 min at 4 °C.

The cell-free lysate was then subjected to ammonium sulfate precipitation on ice, and the amidase was precipitated at 60 and 70% ammonium sulfate saturation as determined by SDS-PAGE. The pellets were resuspended in 20 mM potassium phosphate, pH 7.4, 5 mM DTT.

These fractions were filtered through a 0.45-μm filter and loaded onto to a HiPrep 16/10 Q-Sepharose Fast Flow column (GE Healthcare) equilibrated with 20 mM potassium phosphate, pH 7.4, 5 mM DTT, 100 mM NaCl. The proteins were eluted with a linear gradient of 0.1–1 M NaCl in 20 mM potassium phosphate, 2 mM DTT. Fractions containing the amidase were pooled and concentrated in an Amicon ultrafiltration unit using a 10,000 nominal molecular weight limit polyethersulfone membrane (Millipore, Bedford, MA) under nitrogen pressure.

The concentrated protein sample was then purified to homogeneity by size exclusion chromatography and loaded onto a Sephacryl S-400 gel filtration column (GE Healthcare) equili-

brated with 20 mM Tris, pH 7.4, 2 mM DTT, 150 mM NaCl. Protein purity was assessed by SDS-PAGE and Coomassie Blue staining.

Enzyme Activity Assay—Purified wild-type amidase and the E142L and E142D mutants were assayed for activity by a modified indophenol blue assay utilizing the Berthelot reaction (23). Briefly, 0.08 mg/ml enzyme was incubated in a 1-ml volume of reaction buffer (20 mM potassium phosphate, pH 7.4, 150 mM NaCl, 2 mM dithiothreitol). Substrates were added to a final concentration of 10 mM. This mixture was incubated at 37 °C for 90 min after which ammonia production was detected colorimetrically at 620 nm.

Protein Digestion and MALDI Mass Spectroscopy—Protein samples were diluted to 1 mg/ml in 90-μl aliquots with 100 mM Tris (Fluka). Substrates were added to the samples at a 10-fold molar excess concentration for 30 min before denaturation. To this solution, 10 μl of a mixture of 4 M urea (Sigma) and 300 mM DTT was added to a final concentration of 6 M and 30 mM, respectively. The protein was denatured for 60 min. The digestion mixture was loaded on a 3000 nominal molecular weight-cutoff spin filter (Millipore), and 400 μl of 50 mM ammonium bicarbonate, pH 8 was added. The volume was reduced to 10 μl by centrifugation at 14,000 $\times$ *g* for 100 min. The process was repeated twice, and the final volume was adjusted to 90 μl with 50 mM NH_4HCO_3. Digestion was performed by adding 10 μl of a 0.2 μg/μl trypsin (Applied Biosystems, Germany) solution. The reaction was terminated by adding trifluoroacetic acid (Sigma) to a final concentration of 0.1%. Sample volume was reduced to 10 μl in a SpeedVac vacuum evaporator.

Each sample was fractionated directly onto the MALDI source plate using C_{18} ZipTip® (Millipore) by eluting sequentially with 0.1% TFA, water; 25% acetonitrile, water with 0.1% TFA; 50% acetonitrile, water with 0.1% TFA; and 75% acetonitrile, water with 0.1% TFA (GC grade acetonitrile was supplied by Burdick and Jackson). The eluted compounds were deposited on the source plate in 3–5-μl aliquots. The sample spots were reduced in size by air drying at room temperature before adding 5 μl of 5 mg/ml α-cyano-4-hydroxycinnamic acid (Fluka) matrix.

Mass spectral data were acquired on an Applied Biosystems 4800 MALDI-TOF/TOF instrument. Data were acquired in reflectron positive ion mode with default calibration and the scan range set to *m/z* 800–4000. Spectra were recorded at 50 shots/subspectrum with a total of 1000 spectra. The source voltage was set to 20 kV with the grid voltage at 16 kV. Delayed extraction time was set to 400 ns. Data processing was done with GPS Explorer software from Applied Biosystems.

Protein Crystallization and Data Collection—The purified amidase was crystallized by hanging drop vapor diffusion (22). Briefly, 2 μl of a 10 mg/ml sample of protein was mixed in a 1:1 ratio with the precipitant (1.2 M sodium citrate, 400 mM sodium chloride, 0.1 M sodium acetate, pH 5.6) and allowed to equilibrate by vapor diffusion. Heavily twinned crystals grew after 2 days, and these were used to streak seed-equilibrated drops. Diffraction quality crystals grew after 1 day at room temperature. Crystals were soaked in the well precipitant solution to which a 10-fold molar excess of amide substrate over protein had been added for at least 24 h prior to cryomounting. Crystals were mounted in nylon loops (Hampton) and vitrified by plunging into liquid nitrogen or in the 100 K nitrogen stream of the cryosystem.

Diffraction data were collected using the diffractometer located on beamline BM14 at the European Synchrotron Radiation Facility, Grenoble, France (Protein Data Bank codes 4kzf and 4lf0) and on a Rigaku diffractometer equipped with a Micromax 007HF copper rotating anode, Varimax HF confocal optical system, AFC-11 κ four-circle goniometer, and a Saturn 944+ charge-coupled device camera (Protein Data Bank codes 4gyn and 4gyl). Crystals were maintained at 100 K during data collection, and diffraction images were collected with oscillations about a single axis.

Approximately 80° of data were collected for each crystal of the E142L mutant. In general, only the number of frames necessary to produce a >95% complete data set were integrated and scaled with d*Trek (24). The structures were solved by rigid body refinement with Refmac5 (25) using the wild-type amidase (6) (Protein Data Bank code 2plq) as a model. The structures were refined by a cyclical process involving manual model building with Coot (26) and restrained refinement with Refmac5 (25). In general, no more than two cycles were necessary to achieve convergence as judged by an acceptable fit to the map and the achievement of a minimum value of R_{free} based on 5% of the reflections that were not used in refinement. Analysis of the structures and the molecular graphics diagrams were done with UCSF Chimera (27). The descriptor file for the modified amino acid resulting from the Michael addition of acrylamide to cysteine (*S*-(3-propanamido)cysteine) was created using Sketcher in the CCP4 package. It is reported in the coordinate file as a propionamide linked to Cys-166. The coordinates were deposited in the Protein Data Bank with codes 4lf0 for the E142D mutant of *G. pallidus* amidase enzyme, 4kzf for the E142L mutant enzyme, 4gyn for the E142L mutant enzyme in the presence of propionamide, and 4gyl for the Michael adduct of this mutant enzyme.

Modeling of Substrate in the Wild-type and mutant Enzymes—A two-layer combined quantum mechanics and molecular mechanics (QM/MM)[4] ONIOM (28, 29) calculation was used to study the structure of the active site in E142L. A toolkit to assist ONIOM calculations was used in setting up the calculations from the crystal structure (30). The high level (QM) part of the system was calculated using the B3LYP density functional method (31–34) with a 6-31+G(*d*,*p*) basis set. For the low level (MM) part, the AMBER ff03 force field was used for the enzyme (35, 36), and the generalized AMBER force field (37) with partial charges obtained from a restrained electrostatic potential (37–39) fit to the HF/6-31G(*d*) electron density was used for the acrylamide substrate. A mechanical embedding scheme in which the electrostatic interactions between the high level and low level regions are handled through partial atomic charges in the MM Hamiltonian was used for the geometry optimization. This combined level of theory is commonly denoted ONIOM(B3LYP/6-31+G(*d*,*p*):AMBER). The crystal structure of E142L was used as a starting point for the QM/MM

[4] The abbreviations used are: QM, quantum mechanics; MM, molecular mechanics.

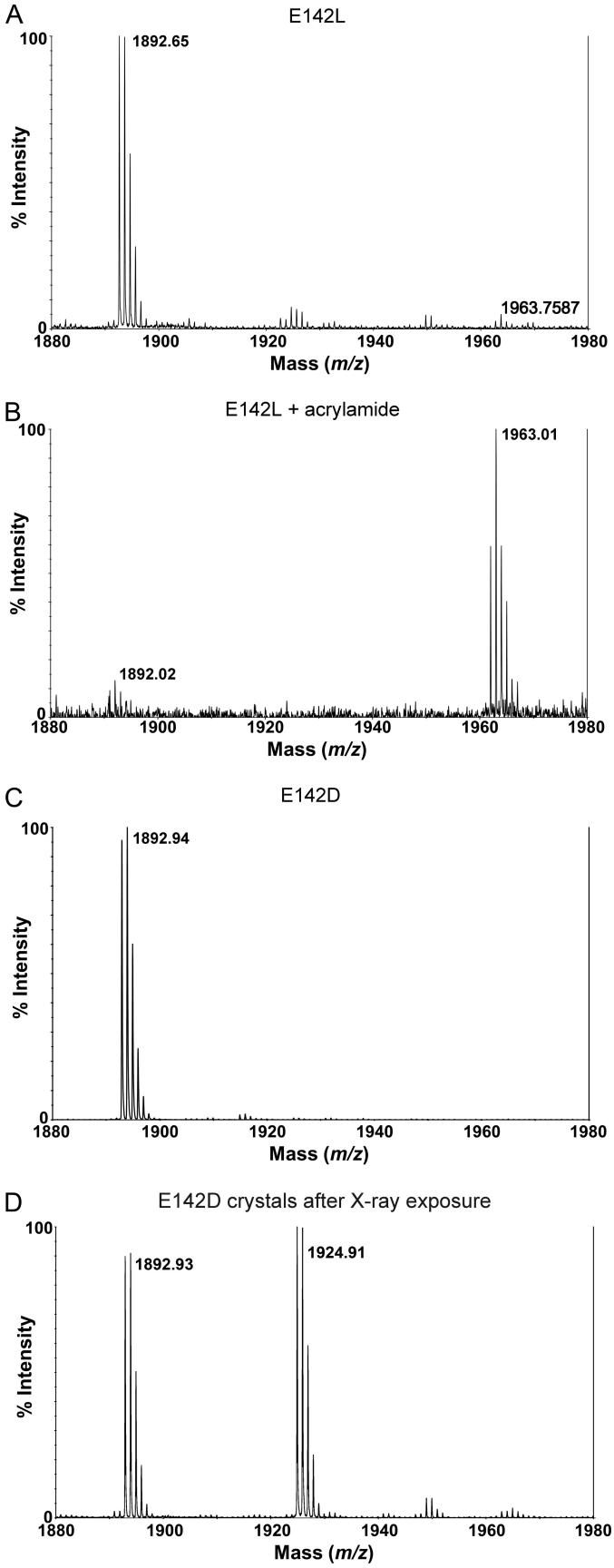

FIGURE 1. **Identification of adduct formation.** Part of the mass spectrum of the tryptic digest of the E142L mutant of the amidase from *G. pallidus* is shown. *A* shows the peak corresponding to the tryptic fragment containing the active site cysteine, Cys-166 (M_r = 1892). *B* shows the decrease in the intensity of the species with M_r = 1892 and a corresponding increase in the intensity of a new species with M_r = 1963. The 71-Da mass increase in this fragment after reaction with acrylamide indicates the formation of a Michael adduct. No other cysteine-containing fragments experienced a mass shift after the reaction. *C*, in the case of the E142D mutant enzyme, only the peak at M_r = 1892 was observed after soaking the crystals in a 10-fold molar excess of the amide substrates. *D*, after exposure, a peak at M_r = 1924 was observed in addition to the peak at M_r = 1892, indicating that a substantial proportion of the cysteine had been converted to cysteine sulfinic acid.

calculations with acrylamide docked in place in the active site in an orientation consistent with the observed reactivity. The Gaussian 09 package was used for all ONIOM and density functional theory calculations (40).

RESULTS

The Enzymatic Activity of the E142L and E142D Mutant Amidases—The known substrates of the amidase from *G. pallidus* RAPc8 are acetamide, acrylamide, lactamide, fluoroacetamide, isobutyramide, formamide, and propionamide (17). The wild-type enzyme was active against all these substrates as demonstrated by ammonia production. However, no ammonia was detected when any of the substrates was incubated with either the E142L mutant or the E142D mutant for 90 min at 37 °C in triplicate repeats. Mutating Glu-142 to either a leucine or an aspartate therefore renders the amidase inactive.

Mass Spectrometry—After reaction with each of the substrates, the E142L and E142D mutant amidases were digested with trypsin, and the masses of the resulting peptides were determined by mass spectroscopy. In particular, an increase in the mass of the peptide that contains the active site cysteine (m/z = 1892) was expected if the predicted thioester intermediate had formed. No changes were observed except in the case of the acrylamide reaction with the E142L mutant (Fig. 1). Relative to the wild-type profile there was a decrease in the intensity of the peak at m/z = 1892, and a new peak at m/z = 1963 was observed. The mass shift of +71 is well known to correspond to the formation of a Michael adduct of acrylamide (M_r = 71) to a cysteine.

The mass spectrometry experiment was repeated on crystals of the E142L and E142D mutant amidases that were soaked in a 10-fold molar excess of substrate. No modifications were observed except in the case of the E142L mutant that had been soaked in acrylamide (Fig. 1*C*). In this case, the result was similar to that described above in that the tryptic fragment containing the active site cysteine was increased in mass by 71 Da relative to the wild-type enzyme. Some of the crystals of the E142D mutant amidase were analyzed after exposure on the synchrotron beamline and showed a peak at m/z = 1924, indicating that the cysteine had been oxidized to cysteine sulfinic acid during the exposure (Fig. 1*D*).

The Crystal Structures of the E142L and E142D Mutants of the Amidase from G. pallidus That Had Been Soaked in Amide Substrates—Diffraction data were collected from six crystals of the E142L mutant of amidase that had not been exposed to any substrate at the European Synchrotron Radiation Facility BM14 beamline. Data from single crystals of both mutants and crystals that had been soaked in one of the substrates (acetamide, isobutyramide, propionamide, fluoroacetamide, or acrylamide)

TABLE 1

Data collection and refinement statistics

ESRF, European Synchrotron Radiation Facility; r.m.s., root mean square.

	E142L + propionamide	E142L + acrylamide	E142L	E142D
Protein Data Bank code	4gyn	4gyl	4kzf	4lf0
Data collection				
X-ray source	Rigaku rotating anode	Rigaku rotating anode	BM14, ESRF	BM14, ESRF
Wavelength (Å)	1.542	1.542	0.9537	0.7749
Temperature (K)	100	100	100	100
Space group	$P4_232$	$P4_232$	$P4_232$	$P4_232$
Oscillation angle (°)	1	0.5	1	0.25
Number of frames	80	200	32	124
Unit cell parameter (Å)	$a = 130.79$	$a = 130.49$	$a = 130.89$	$a = 130.63$
Resolution range (Å)	53.39–1.90 (1.97–1.90)	24.23–1.90 (1.97–1.90)	36.30–1.84	53.3–1.101 (1.106–1.101)
Mosaicity (°)	0.22	0.23	1.10	0.066
No. of observed reflections	164,555	486,668	221,828	1,139,394
No. of unique reflections	29,066	30,455	33,703	152,140
No. of unique reflections in test set	1,446	1,533	1,654	7,512
Completeness (%)	94.6 (93.7)	99.9 (99.1)	99.7 (99.5)	99.8 (99.5)
Multiplicity	5.66 (5.09)	15.98 (6.56)	6.58 (4.87)	7.49 (7.46)
$I/\sigma(I)$	5.0 (2.3)	7.8 (2.1)	10.6 (2.8)	34.5 (11.2)
Wilson B factor (Å^2)	24.9	28.3	29.5	8.6
R_{meas} [a]	0.225 (0.516)	0.253 (0.688)	0.087 (0.526)	0.043 (0.20)
No. of protein molecules in asymmetric unit	1	1	1	1
Matthews coefficient, V_M (Å^3 Da^{-1})	2.5	2.5	2.5	2.43
Solvent content (%)	50	50	50	48.9
Refinement				
Resolution range (Å)	53.39–1.90	24.23 − 1.90	36.30–1.84	53.3–1.10
Contents of asymmetric unit (excluding hydrogen atoms)				
No. of protein atoms	2,661	2,659	2,661	2,661
No. of chloride ions	1	1	1	0
No. of water atoms	213	243	205	386
Average B factor (Å^2)	14.5	17.5	28.7	7.63
r.m.s. deviations from ideal				
Bond lengths (Å)	0.019	0.022	0.028	0.025
Bond angles (°)	1.41	2.08	2.28	2.28
Ramachandran favored	319	319	317	324
Ramachandran allowed	16	16	15	13
Ramachandran outliers	3	3	3	1
R_{cryst} [b]	0.17 (0.23)	0.17 (0.19)	0.20	0.145
R_{free} [c]	0.20 (0.27)	0.19 (0.21)	0.22	0.149

[a] $R_{meas} = \Sigma_{hkl}[n/(n-1)]^{1/2}\Sigma_i|I_i(hkl) - I(hkl)|/\Sigma_{hkl}\Sigma_i I_i(hkl)$ where $I_i(hkl)$ is the ith measurement of the intensity of reflection hkl, $I(hkl)$ is the mean intensity of reflection hkl, and n is the number of observations of intensity $I(hkl)$ (multiplicity) (20).

[b] $R_{cryst} = \Sigma_{hkl}||F_{obs}| - |F_{calc}||/\Sigma_{hkl}|F_{obs}|$ where F_{obs} and F_{calc} are the observed and calculated structure factors, respectively.

[c] R_{free} was calculated analogously for a randomly selected 5% of the reflections. The numbers in parentheses indicate the values for the highest resolution shell.

were collected on a diffractometer with a copper rotating anode source. All the crystals had the same space group symmetry ($P4_232$ with one molecule in the asymmetric unit) and similar unit cell parameters as the wild-type *G. pallidus* RAPc8 amidase structure (6) (Protein Data Bank code 2plq). Data collection and refinement statistics for four crystals are shown in Table 1.

The structure of the E142L amidase mutant shows that the geometry of the active site is maintained (Fig. 2*A*), in particular the locations of the "catalytic triad": Cys-166, Lys-134, and Glu-59 are identical to those in the wild-type enzyme (Fig. 2*B*). The leucine side chain of the mutant is slightly displaced from the location of the glutamate in the wild-type enzyme (Fig. 3*A*). There is no significant movement of the backbone atoms in the vicinity of the active site. The leucine side chain is located in poorly defined density, suggesting that there are no interactions to constrain its position. Also the loop 139–143 is clearly more mobile as the density in this region, which is well defined in the wild-type enzyme, is broken up and disconnected in some of the mutant crystal structures. This is also shown by the increase in the atomic temperature factors in this region of the model (Fig. 4*A*).

A chloride ion is located 2.9 Å from Lys-134 N^{ζ} and 2.8 Å from the backbone amide nitrogen of Trp-138 (Fig. 4*B*). These interactions contribute to the stabilization of the loop. This chloride ion occupies the same position as Glu-142 $O^{\epsilon 1}$ in the wild-type enzyme. There is no atom in the location of the Glu-142 $O^{\epsilon 2}$. The Glu-142 $O^{\epsilon 2}$-equivalent atom is hydrogen bonded to the substrate amino group in the C165A mutant of the carbamoylase from *A. radiobacter* (16). This same Glu-142 $O^{\epsilon 2}$ atom forms a hydrogen bond with Tyr-60 O^{η} in the wild-type enzyme, but despite the absence of this interaction, the location of Tyr-60 is almost unchanged in the mutant. In the case of the mutant crystals that had been soaked in propionamide, there was no density connected to the Cys-166 S^{γ}, but there were two nearby, but separated, spheres of density that were interpreted as water molecules (Fig. 3*A*).

There was additional density connected to that of the S^{γ} of Cys-166 in the structure determined from every crystal except those of the E142L mutant enzyme that had been soaked in propionamide and isobutyramide (Fig. 5). With the exception of the density seen in the case of the acrylamide-soaked crystal, which is discussed in detail below, this density resembled that seen in the wild-type structure described by Kimani *et al.* (6)

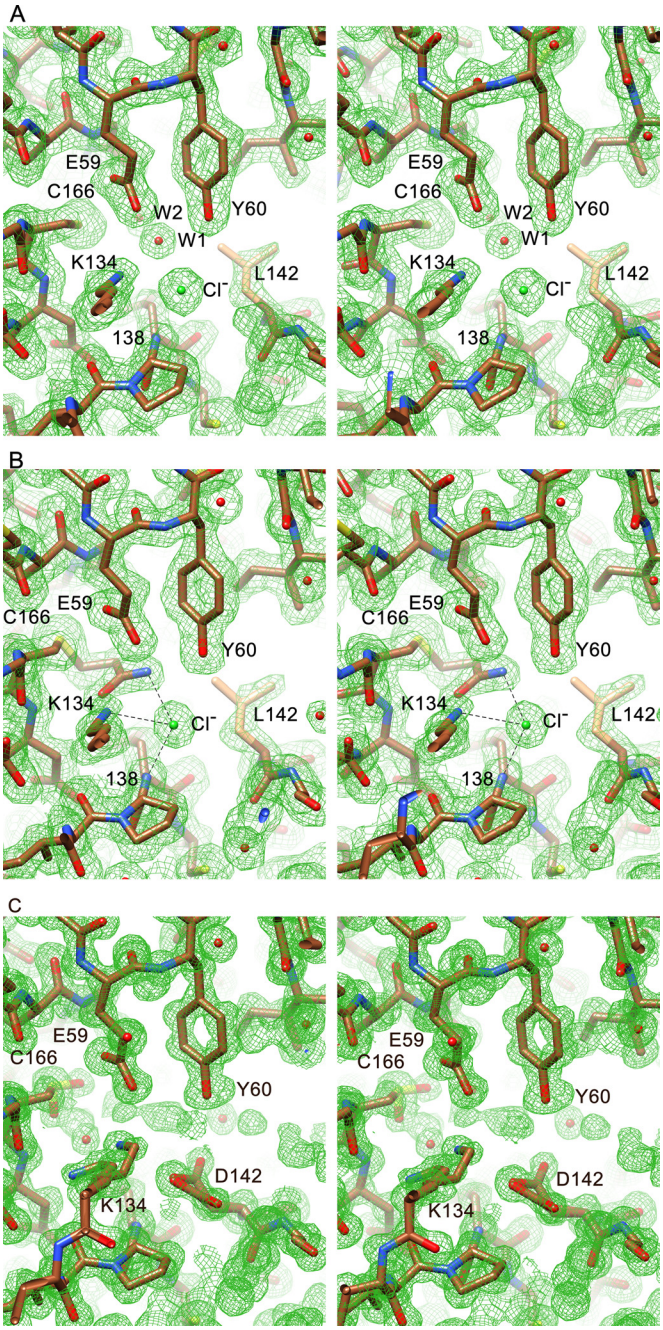

FIGURE 2. **The active sites of the E142L and E142D mutants.** *A*, electron density map of the E142L mutant of the amidase from *G. pallidus* RAPc8 contoured at 1.0 σ. Three distinct spheres of density in the active site are interpreted as a chloride ion and two water molecules (*W1* and *W2*). The chloride ion is 2.9 Å from the amino group nitrogen of Lys-134 and 2.9 Å from the backbone amino group of Trp-138 (labeled *138*). *B*, the electron density map of the corresponding volume of the E142L mutant after the reaction of the amidase with acrylamide. A Michael adduct is formed with Cys-166. The amide nitrogen of the adduct is located 2.9 Å from the chloride, which in turn moves slightly further away from the mean position of the Lys-134 N^{ζ} (3.1 Å). There is a close contact between the lysine 134 N^{ζ} and the carbonyl oxygen of the adduct, resulting in both atoms having lower than expected electron densities. The distance between the mean locations of these two atoms is 2.1 Å. *C*, the electron density map of the corresponding volume of the E142D mutant enzyme suggests two alternative locations for both Asp-142 and Lys-134. The $O^{\delta 1}$ atom of Asp-142 occupies the same location as Glu-142 $O^{\epsilon 1}$ in the wild-type enzyme, whereas the Asp-142 $O^{\delta 2}$ atom occupies one of two well defined locations. The electron density for Lys-134 is poorly defined and difficult to interpret unambiguously. The density for Cys-166 was best interpreted by assigning occupancies of 0.6 to the two oxygen atoms of cysteine sulfinic acid. Significant density in the vicinity of the active site, presumed to be due to mobile water molecules, could not be interpreted.

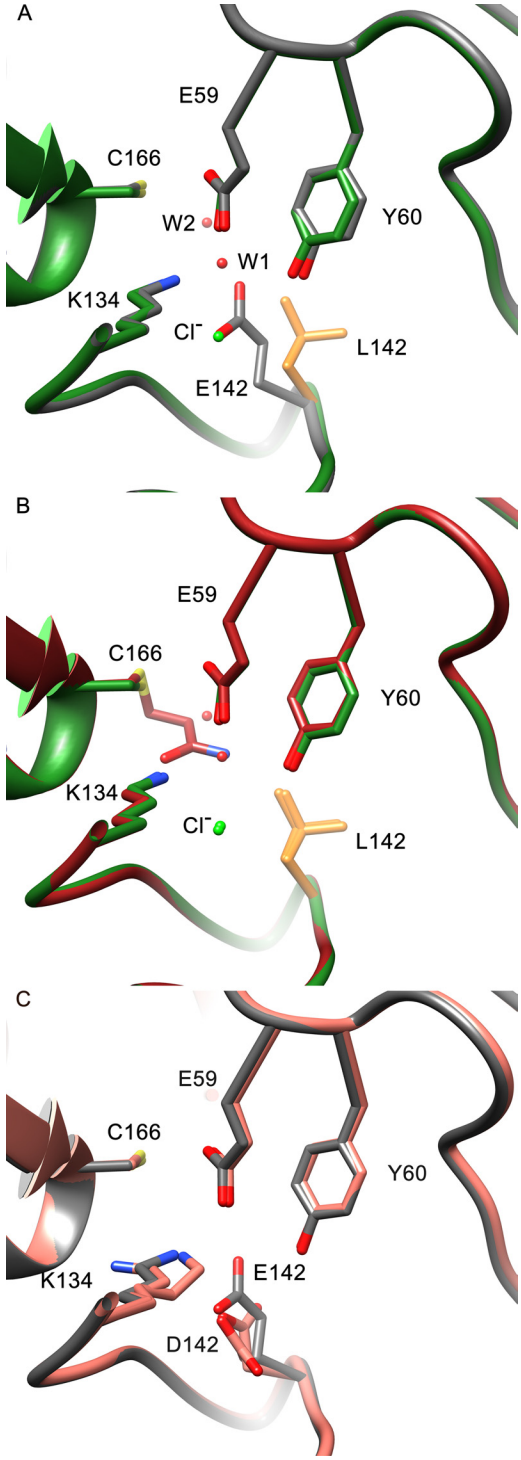

FIGURE 3. **A comparison of the active site of the wild-type enzyme with those of the E142L and E142D mutants.** *A*, a superposition of the active site residues of the wild-type and mutant (E142L) amidase enzymes. The geometry of the common active site residues, Cys-166, Lys-134, Glu-59, and Tyr-60, is maintained. A chloride ion in the E142L mutant occupies the same position as the Glu-142 $O^{\epsilon 1}$ in the wild-type enzyme. The position of Leu-142 is displaced from the position originally occupied by Glu-142. *B*, a superposition of the E142L mutant amidase before and after reaction with acrylamide. The amide oxygen of the Michael adduct at Cys-166 after incubation with acrylamide is in close contact with Lys-134. The two water molecules, *W1* and *W2*, are displaced by the adduct. *C*, the superposition of the active sites of the E142D mutant and the wild-type amidase. Asp-142 $O^{\delta 1}$ occupies the same location as Glu-142 $O^{\epsilon 1}$, but the location of Asp-142 $O^{\delta 2}$ is ambiguous, and in neither case is it the same as that of Glu-142 $O^{\epsilon 2}$.

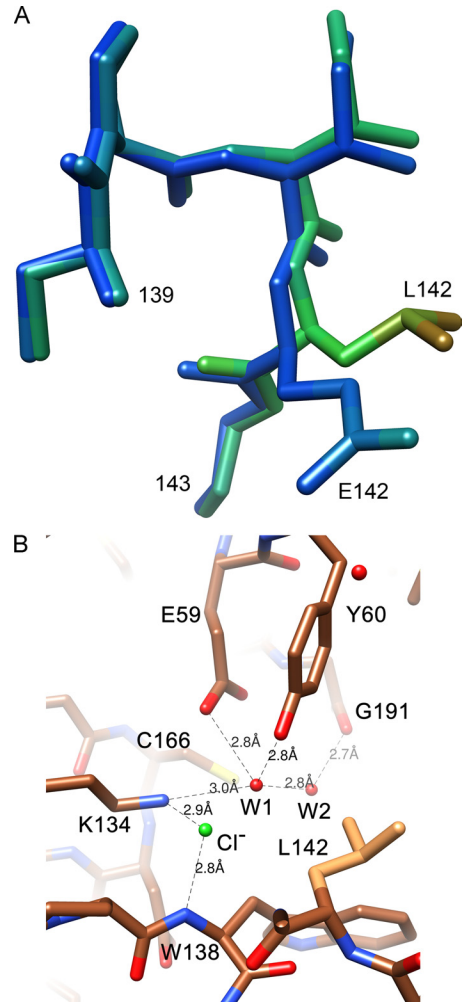

FIGURE 4. **Stabilization of loop 139–143.** *A*, a superposition of residues in the loop 139–143 from the wild-type enzyme and the E142L mutant enzyme colored according to atomic temperature factors in UCSF Chimera. In the wild-type amidase, the position of the loop is constrained by the interactions of Glu-142 with Lys-134 and Tyr-60 and has low temperature factors. In the E142L mutant enzyme, these constraints are absent, and thus, the loop is more flexible as evidenced by the increased temperature factors. The rendering of the temperature factors utilizes a continuous color spectrum in which *dark blue* has a value of 3 Å^2, *green* has a value of 18 Å^2, and *red* 35 has a value of Å^2. *B*, in the E142L mutant, some stabilization of the loop is achieved through interactions with the chloride ion. The chloride ion is positioned 2.8 Å from the backbone amide nitrogen of Trp-138 and 2.9 Å from Lys-134 N$^{\zeta}$. *W1* and *W2*, water molecules.

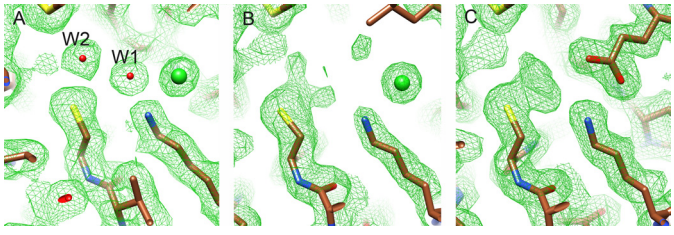

FIGURE 5. **Cysteine oxidation.** Shown is the electron density shown at 0.6 σ surrounding Cys-166 in the map obtained using data collected from a crystal of the E142L mutant of the amidase that had been soaked in propionamide (Protein Data Bank code 4gyn) (*A*), the map obtained using the first 32 frames of data collected from a crystal of the E142L mutant of the amidase (Table 1, column 3) (*B*), and the map obtained from a crystal of wild-type amidase (Protein Data Bank code 2plq) (*C*). The oxygens of the water molecules, *W1* and *W2*, depicted in *A* are located as follows: W1, 3.2 Å from Cys-166 S$^{\gamma}$ and 2.7 Å from the backbone carbonyl oxygen of Gly-191; W2, 2.9 Å from Lys-134 N$^{\zeta}$ and 2.8 Å from Tyr-60 O$^{\eta}$. W2 is 4.0 Å from Cys-166 S$^{\gamma}$.

(Fig. 3*C*). Essentially, electron density connected with that of the sulfur extends into the oxyanion hole (18). The crystals of the E142D mutant amidase were exceptional diffractors that enabled most of the molecule to be visualized at atomic resolution. The density in the vicinity of the active site cysteine was similar to that seen in the E142L mutant amidase crystals. The mass spectroscopy experiment described above confirms that the oxidation of the sulfur occurs in the x-ray beam and indicates that the oxidized species is cysteine sulfinic acid. However, the density did not allow for an unambiguous interpretation.

To minimize this effect, we solved the structure of the E142L mutant enzyme based on only the first 32 frames and found that this density was substantially reduced (Fig. 3*B*). Similar attempts to minimize the effect in the case of the E142D mutant amidase were unsuccessful. We were able to generate a complete data set by utilizing only the first four frames of five different crystals. Despite this, the density was unchanged, indicating that the oxidation occurs rapidly in the case of this mutant. There was density that could be accounted for by four to eight atoms in close proximity to the cysteine. In the absence of any alternative explanation, it is assumed that in addition to the cysteine oxidation the density is due to water molecules in a number of overlapping positions.

In the case of the E142D mutant, both Asp-142 and Lys-134 showed evidence of adopting two alternate conformations. In both conformations of Asp-142, O$^{\delta 1}$ is located in the same position as Glu-142 O$^{\epsilon 1}$ in the wild-type enzyme. In the "A" location, Asp-142 O$^{\delta 2}$ is 3.0 Å from the backbone amide of Trp-144, and in the "B" location, Asp-142 O$^{\delta 2}$ is 2.7 Å from a well defined water molecule. These hydrogen bonding interactions provide a plausible explanation for the two alternate conformations. Indeed, molecular dynamics simulations starting with Asp-142 in the A location readily flipped to the B location once a water molecule moved into the crystallographically observed position (supplemental video). Some poorly defined density was seen at location of Glu-142 O$^{\epsilon 2}$ in the wild-type enzyme, but this was not interpreted.

No substrate molecules could be clearly identified in the maps resulting from the crystals soaked in acetamide, isobutyramide, propionamide, and fluoroacetamide. However, the density at Cys-166 in the structure determined from the E142L mutant amidase crystal soaked in acrylamide showed the product of a Michael addition (Fig. 2*B*), thus confirming the mass spectrometry results (Fig. 1). The two water molecules, W1 and W2, that were located in the proximity of Cys-166 were displaced by the Michael adduct. The amide nitrogen was located close to Glu-59 O$^{\epsilon 2}$ (2.8 Å), Tyr-60 O$^{\eta}$ (2.8 Å), and the Cl^- (2.8 Å). Both the carbonyl oxygen and Lys-134 N$^{\zeta}$ were located in unexpectedly low density below the 2.0 σ contour level possibly because of instability in their positions resulting from their close contact (2.0 Å). The locations of all other atoms in the adduct active site were unchanged (Fig. 3*B*).

Modeling the Substrate Location—An explanation of the docking of the acrylamide substrate leading to the formation of a Michael adduct was sought by modeling using ONIOM with the substrate and first shell of atoms around the active site modeled quantum mechanically. In the case of substrate positioned

TABLE 2

Mean distances between the substrate amide nitrogen, carbon, and oxygen atoms and the key active site residues (Glu^1, Glu^2, Lys, and Cys)

The backbone NH is that of the residue immediately following the active site cysteine. Glu^1 is the residue equivalent to Glu-59, and Glu^2 is the residue equivalent to Glu-142. N/A, not applicable.

	C166S mutant of AmiF from *H. pylori*	C171A mutant of the carbamoylase from *Agrobacterium* sp.	ONIOM model of acrylamide bound to the wild-type amidase	ONIOM model of acrylamide bound to the E142L mutant amidase
	Å	Å	Å	Å
N . . . Glu^1 $O^{\epsilon 2}$	2.9	3.0	2.8	3.6
N . . . Glu^2 $O^{\epsilon 2}$	3.1	3.4	3.0	N/A
N . . . Cl^-	N/A	N/A	N/A	3.0
C . . . Cys C^{β}	3.5	3.4	3.6	3.6
C . . . Cys S^{γ}	N/A	N/A	3.1	3.2
O . . . Lys N^{ζ}	3.3	2.8	2.7	2.6
O . . . NH	3.1	3.2	3.2	3.2

in the wild-type enzyme, the distances between the active site atoms and the amide moiety predicted by the ONIOM calculations are comparable with those observed in the deposited crystal structures of two comparable enzymes in which the active site cysteine is mutated to either a serine or an alanine (Table 2). The quantum-mechanical model places the carbonyl oxygen in the oxyanion hole formed by Lys-134 and the backbone amide group of Asp-167 in both the wild type and the E142L mutant. The amino group, however, instead of being located between the carboxyl oxygens of the two active site glutamates is drawn toward the chloride ion in the E142L mutant enzyme. This is achieved by pivoting around the carbonyl oxygen, thereby altering the orientation of the amide moiety by more than 60° and bringing the acrylamide C^{β} to within 2.2 Å of the S^{γ} of Cys-166 (Fig. 6).

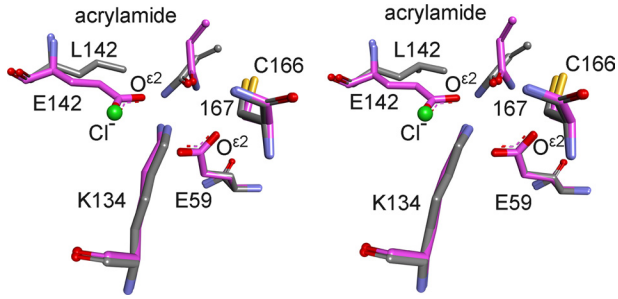

FIGURE 6. **Acrylamide docking using ONIOM.** The formation of the Michael adduct in the E142L mutant enzyme is explained by QM/MM modeling of the acrylamide in the active site pocket of the wild-type enzyme, depicted with *magenta* carbon atoms, superimposed on the mutant, depicted with *gray* carbon atoms. In the mutant enzyme, the acrylamide pivots around the carbonyl oxygen, which is located in the oxyanion hole formed by Lys-134 and the backbone amide of Asp-167 (labeled *167*) as the amino group is drawn toward the chloride ion. In this conformation, the acrylamide C^{β} is positioned close to the S^{γ} of Cys-166, and the stereoelectronic alignment, which is essential for the nucleophilic attack on the carbonyl carbon, is lost.

DISCUSSION

It is clear that Glu-142 plays an essential role in the mechanism of the amidases. Our experiments have helped to define part of this role by demonstrating that, without it, the active site is destabilized in the case of the E142D mutant, or the substrate is mispositioned in the active site in the case of the E142L mutant. The latter point is illustrated by the successful formation of a Michael adduct with acrylamide as a result of positioning the double bond close to the active site cysteine and the failure to react in any way with all the other substrates tested. This suggests that the position of Glu-142 $O^{\epsilon 2}$ in the wild-type enzyme is an essential part of an amide-positioning motif also comprising Lys-134 N^{ζ}, Glu-59 $O^{\epsilon 2}$, and possibly Tyr-60 O^{η}, which is hydrogen bonded to Glu-59 $O^{\epsilon 2}$. It is also clear from our experiment that the hydrogen bond between Glu-142 $O^{\epsilon 2}$ and Lys-134 N^{ζ} assists in stabilizing the loop that contains residues 139–142. Further contributions that Glu-142 may make to the chemistry of the active site, such as raising the pK_a of Lys-134, are not addressed by our experiment. An additional experimental complication occurs as a result of the propensity of Cys-166 to oxidize readily in the x-ray beam. This phenomenon obscures the accurate location of the water molecules in the active site.

Our initial hypothesis was that Glu-142 acts as a general base catalyst in the second part of the ping-pong bi-bi sequence. That is, it enhances the nucleophilicity of the second substrate, assisting its attack on the carbonyl carbon of the thioester. The second substrate is usually water but could also be hydroxylamine in the case of an acyl transfer reaction. According to this hypothesis, replacing Glu-142 with a leucine would enable the visualization of the thioester intermediate. Mass spectroscopic evidence in the case of the *Rhodococcus* ATCC 39484 nitrilase suggests that either the thioimidate or the thioester forms a stable intermediate in the case of poor nitrile substrates (19). No evidence for the formation of the thioester was found in the case of the amidase for any of the substrates we tested. Therefore, our initial hypothesis was not confirmed directly. However, it is not disproved either because of the substantial mispositioning of the substrate in the modified enzyme.

The first part of the reaction involving a nucleophilic attack by the active site cysteine (Cys-166) on the substrate carbonyl carbon did not occur. Instead, in the case of the E142L mutant, the cysteine attacked the terminal carbon (C^{β}) of the acrylamide. This could only come about as a result of mispositioning the amide moiety so that an attack on the carbonyl carbon was no longer favored. This is demonstrated by the formation of the Michael adduct with the acrylamide substrate. In addition, no amidase reaction occurred with any of the substrates tested with either the E142L or E142D mutant enzyme. In both of these mutants, the "anion hole" located between Lys-134 N^{ζ} and the backbone amide of Trp-138 that is normally occupied by Glu-142 $O^{\epsilon 1}$ was occupied by an anion, but the location normally occupied by the Glu-142 $O^{\epsilon 2}$ was vacant. This atom hydrogen bonds to the substrate amino group, and our result demonstrates the key role it plays in correctly positioning the substrate. Docking using a QM/MM protocol strengthens this hypothesis and suggests the plausibility of an assisted Michael addition as depicted in Fig. 7. It has frequently been suggested

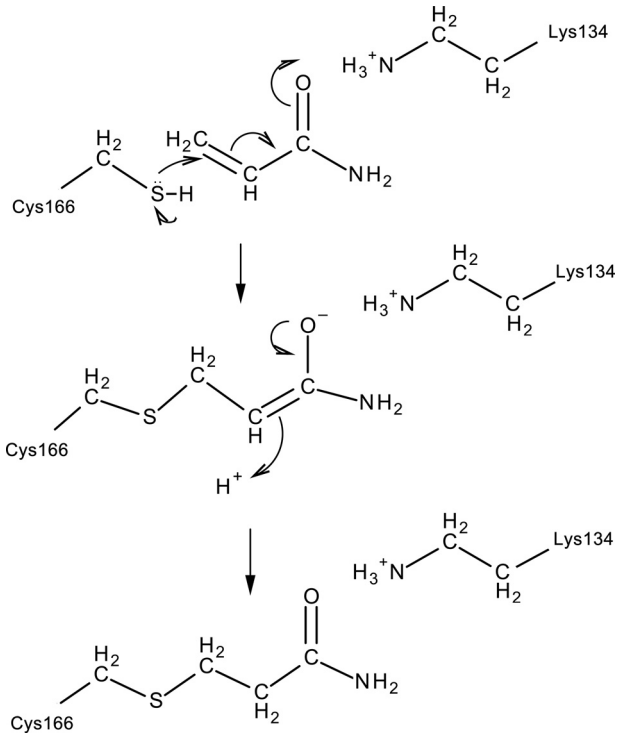

FIGURE 7. **Proposed reaction scheme for the formation of the Michael adduct.** The nucleophilic sulfur of Cys-166 of the E142L mutant attacks the acrylamide at the terminal carbon or β-carbon instead of the carbonyl carbon due to the mispositioning of the amide group in the active site. The positive charge of Lys-134 transiently stabilizes the enolate intermediate, which subsequently collapses, resulting in the formation of a stable Michael adduct at Cys-166. Our experiment does not provide insight into which base transiently binds the proton, but it could possibly be Glu-59.

that the nucleophilic attack is assisted by base catalysis involving Glu-59. This could potentially occur either in the normally occurring formation of the thioester or in the formation of the Michael adduct as occurs in the E142L mutant. Stereoelectronic considerations dictate the trajectory of the nucleophilic attack in the case of the wild-type enzyme. Specifically, the lone pair of the Cys-166 S^{γ} must overlap with the π^* antibonding orbital of the substrate carbon to proceed to a stable transition state. Visualization of the details of the state immediately prior to the nucleophilic attack cannot be achieved using x-ray crystallography. The closest approximation that has been achieved involves substitution of an alanine or serine for the active site cysteine. We have not accomplished this for the *G. pallidus* amidase, but it has been done for a closely related amidase (9) and carbamoylase (16), enabling us to model the location of the acrylamide in the active site of the wild-type *G. pallidus* amidase.

Our experiment emphasizes the importance of colinear alignment in the transition state of the sulfhydryl *p* orbital with that of the amide lowest unoccupied molecular orbital as a prerequisite for the reaction. The models show how the EKE triad together with the backbone atoms, including the peptidic amide of Asp-167 and the peptidic carbonyl of Gly-191, provide a specific amide recognition motif that acts much like a vice to position the amide lowest unoccupied molecular orbital. We have shown that without correct substrate positioning brought about *inter alia* by interactions with Glu-142 $O^{\epsilon 2}$ the thioester will not form. The study of the catalytic role of Glu-142 in the hydrolysis of the thioester is therefore precluded in the experiment we performed, and it will be necessary to prove the details of its involvement in other ways.

Acknowledgments—We thank the Centre for High Performance Computing for use of resources. We thank Dr. Hassan Belrhali of European Molecular Biology Laboratory, Grenoble, France for giving us access to the BM14 beamline at European Synchrotron Radiation Facility; Professor Wolf-Dieter Schubert for giving us access to the diffractometer at the University of the Western Cape; and Professor Heinrich Dirr and Dr. Manuel Fenandes for giving us access to the diffractometer at the University of the Witwatersrand. We thank Dr. Mare Vlok for obtaining the mass spectra.

REFERENCES

1. Chien, C. H., Gao, Q. Z., Cooper, A. J., Lyu, J. H., and Sheu, S. Y. (2012) Structural insights into the catalytic active site and activity of human Nit2/ω-amidase: kinetic assay and molecular dynamics simulation. *J. Biol. Chem.* **287,** 25715–25726
2. Krasnikov, B. F., Chien, C. H., Nostramo, R., Pinto, J. T., Nieves, E., Callaway, M., Sun, J., Huebner, K., and Cooper, A. J. (2009) Identification of the putative tumor suppressor Nit2 as ω-amidase, an enzyme metabolically linked to glutamine and asparagine transamination. *Biochimie* **91,** 1072–1080
3. Bork, P., and Koonin, E. V. (1994) A new family of carbon-nitrogen hydrolases. *Protein Sci.* **3,** 1344–1346
4. Pace, H. C., and Brenner, C. (2001) The nitrilase superfamily: classification, structure and function. *Genome Biol.* **2,** REVIEWS0001
5. Soriano-Maldonado, P., Martínez-Gómez, A. I., Andújar-Sánchez, M., Neira, J. L., Clemente-Jiménez, J. M., Las Heras-Vázquez, F. J., Rodríguez-Vico, F., and Martínez-Rodríguez, S. (2011) Biochemical and mutational studies of the *Bacillus cereus* CECT 5050T formamidase support the existence of a C-E-E-K tetrad in several members of the nitrilase superfamily. *Appl. Environ. Microbiol.* **77,** 5761–5769
6. Kimani, S. W., Agarkar, V. B., Cowan, D. A., Sayed, M. F., and Sewell, B. T. (2007) Structure of an aliphatic amidase from *Geobacillus pallidus* RAPc8. *Acta Crystallogr. D Biol. Crystallogr.* **63,** 1048–1058
7. Nel, A. J., Tuffin, I. M., Sewell, B. T., and Cowan, D. A. (2011) Unique aliphatic amidase from a psychrotrophic and haloalkaliphilic *Nesterenkonia* isolate. *Appl. Environ. Microbiol.* **77,** 3696–3702
8. Thuku, R. N., Brady, D., Benedik, M. J., and Sewell, B. T. (2009) Microbial nitrilases: versatile, spiral forming, industrial enzymes. *J. Appl. Microbiol.* **106,** 703–727
9. Hung, C. L., Liu, J. H., Chiu, W. C., Huang, S. W., Hwang, J. K., and Wang, W. C. (2007) Crystal structure of *Helicobacter pylori* formamidase AmiF reveals a cysteine-glutamate-lysine catalytic triad. *J. Biol. Chem.* **282,** 12220–12229
10. Maestracci, M., Thiery, A., Arnaud, A., and Galzy, P. (1986) A study of the mechanism of the reactions catalyzed by the amidase *Brevibacterium* sp. R312. *Agr. Biol. Chem. Tokyo* **50,** 2237–2241
11. Nakai, T., Hasegawa, T., Yamashita, E., Yamamoto, M., Kumasaka, T., Ueki, T., Nanba, H., Ikenaka, Y., Takahashi, S., Sato, M., and Tsukihara, T. (2000) Crystal structure of N-carbamyl-D-amino acid amidohydrolase with a novel catalytic framework common to amidohydrolases. *Structure* **8,** 729–737
12. Fernandes, B. C., Mateo, C., Kiziak, C., Chmura, A., Wacker, J., van Rantwijk, F., Stolz, A., and Sheldon, R. A. (2006) Nitrile hydratase activity of a recombinant nitrilase. *Adv. Synth. Catal.* **348,** 2597–2603
13. Jandhyala, D. M., Willson, R. C., Sewell, B. T., and Benedik, M. J. (2005) Comparison of cyanide-degrading nitrilases. *Appl. Microbiol. Biotechnol.* **68,** 327–335
14. Piotrowski, M. (2008) Primary or secondary? Versatile nitrilases in plant metabolism. *Phytochemistry* **69,** 2655–2667
15. Andrade, J., Karmali, A., Carrondo, M. A., and Frazão, C. (2007) Structure

of amidase from *Pseudomonas aeruginosa* showing a trapped acyl transfer reaction intermediate state. *J. Biol. Chem.* **282,** 19598–19605
16. Chen, C. Y., Chiu, W. C., Liu, J. S., Hsu, W. H., and Wang, W. C. (2003) Structural basis for catalysis and substrate specificity of *Agrobacterium radiobacter N*-carbamoyl-D-amino acid amidohydrolase. *J. Biol. Chem.* **278,** 26194–26201
17. Makhongela, H. S., Glowacka, A. E., Agarkar, V. B., Sewell, B. T., Weber, B., Cameron, R. A., Cowan, D. A., and Burton, S. G. (2007) A novel thermostable nitrilase superfamily amidase from *Geobacillus pallidus* showing acyl transfer activity. *Appl. Microbiol. Biotechnol.* **75,** 801–811
18. Raczynska, J. E., Vorgias, C. E., Antranikian, G., and Rypniewski, W. (2011) Crystallographic analysis of a thermoactive nitrilase. *J. Struct. Biol.* **173,** 294–302
19. Stevenson, D. E., Feng, R., and Storer, A. C. (1990) Detection of covalent enzyme-substrate complexes of nitrilase by ion-spray mass spectroscopy. *FEBS Lett.* **277,** 112–114
20. Diederichs, K., and Karplus, P. A. (1997) Improved R-factors for diffraction data analysis in macromolecular crystallography. *Nat. Struct. Biol.* **4,** 269–275
21. Cameron, R. A., Sayed, M., and Cowan, D. A. (2005) Molecular analysis of the nitrile catabolism operon of the thermophile *Bacillus pallidus* RAPc8. *Biochim. Biophys. Acta* **1725,** 35–46
22. Agarkar, V. B., Kimani, S. W., Cowan, D. A., Sayed, M. F., and Sewell, B. T. (2006) The quaternary structure of the amidase from *Geobacillus pallidus* RAPc8 is revealed by its crystal packing. *Acta Crystallogr. Sect. F Struct. Biol. Cryst. Commun.* **62,** 1174–1178
23. Horn, D. B., and Squire, C. R. (1966) Estimation of ammonia using indophenol blue reaction. *Clin. Chim. Acta* **14,** 185–194
24. Pflugrath, J. W. (1999) The finer things in x-ray diffraction data collection. *Acta Crystallogr. D Biol. Crystallogr.* **55,** 1718–1725
25. Murshudov, G. N., Vagin, A. A., and Dodson, E. J. (1997) Refinement of macromolecular structures by the maximum-likelihood method. *Acta Crystallogr. D Biol. Crystallogr.* **53,** 240–255
26. Emsley, P., Lohkamp, B., Scott, W. G., and Cowtan, K. (2010) Features and development of Coot. *Acta Crystallogr. D Biol. Crystallogr.* **66,** 486–501
27. Pettersen, E. F., Goddard, T. D., Huang, C. C., Couch, G. S., Greenblatt, D. M., Meng, E. C., and Ferrin, T. E. (2004) UCSF Chimera—a visualization system for exploratory research and analysis. *J. Comput. Chem.* **25,** 1605–1612
28. Dapprich, S., Komaromi, I., Byun, K. S., Morokuma, K., and Frisch, M. J. (1999) A new ONIOM implementation in Gaussian98. Part I. The calculation of energies, gradients, vibrational frequencies and electric field derivatives. *Theochem* **461,** 1–21
29. Vreven, T., Byun, K. S., Komaromi, I., Dapprich, S., Montgomery, J. A., Morokuma, K., and Frisch, M. J. (2006) Combining quantum mechanics methods with molecular mechanics methods in ONIOM. *J. Chem. Theory Comput.* **2,** 815–826
30. Tao, P., and Schlegel, H. B. (2010) A toolkit to assist ONIOM calculations. *J. Comput. Chem.* **31,** 2363–2369
31. Vosko, S. H., Wilk, L., and Nusair, M. (1980) Accurate spin-dependent electron liquid correlation energies for local spin-density calculations—a critical analysis. *Can. J. Phys.* **58,** 1200–1211
32. Becke, A. D. (1993) Density-functional thermochemistry. 3. The role of exact exchange. *J. Chem. Phys.* **98,** 5648–5652
33. Lee, C., Yang, W., and Parr, R. G. (1988) Development of the Colle-Salvetti correlation-energy formula into a functional of the electron density. *Phys. Rev. B Condens. Matter* **37,** 785–789
34. Stephens, P. J., Devlin, F. J., Chabalowski, C. F., and Frisch, M. J. (1994) Ab initio calculation of vibrational absorption and circular-dichroism spectra using density functional force fields. *J. Phys. Chem.* **98,** 11623–11627
35. Duan, Y., Wu, C., Chowdhury, S., Lee, M. C., Xiong, G., Zhang, W., Yang, R., Cieplak, P., Luo, R., Lee, T., Caldwell, J., Wang, J., and Kollman, P. (2003) A point-charge force field for molecular mechanics simulations of proteins based on condensed-phase quantum mechanical calculations. *J. Comput. Chem.* **24,** 1999–2012
36. Lee, M. C., and Duan, Y. (2004) Distinguish protein decoys by using a scoring function based on a new AMBER force field, short molecular dynamics simulations, and the generalized born solvent model. *Proteins* **55,** 620–634
37. Wang, J., Wolf, R. M., Caldwell, J. W., Kollman, P. A., and Case, D. A. (2004) Development and testing of a general amber force field. *J. Comput. Chem.* **25,** 1157–1174
38. Bayly, C. I., Cieplak, P., Cornell, W. D., and Kollman, P. A. (1993) A well-behaved electrostatic potential based method using charge restraints for deriving atomic charges—the RESP model. *J. Phys. Chem.* **97,** 10269–10280
39. Cornell, W. D., Cieplak, P., Bayly, C. I., and Kollman, P. A. (1993) Application of RESP charges to calculate conformational energies, hydrogen bond energies and free energies of solvation. *J. Am. Chem. Soc.* **115,** 9620–9631
40. Frisch, M. J., Trucks, G. W., Schlegel, H. B., Scuseria, G. E., Robb, M. A., Cheeseman, J. R., Scalmani, G., Barone, V., Mennucci, B., Petersson, G. A., Nakatsuji, H., Caricato, M., Li, X., Hratchian, H. P., Izmaylov, A. F., Bloino, J., Zheng, G., Sonnenberg, J. L., Hada, M., Ehara, M., Toyota, K., Fukuda, R., Hasegawa, J., Ishida, M., Nakajima, T., Honda, Y., Kitao, O., Nakai, H., Vreven, T., Montgomery, J. A., Jr., Peralta, J. E., Ogliaro, F., Bearpark, M., Heyd, J. J., Brothers, E., Kudin, K. N., Staroverov, V. N., Kobayashi, R., Normand, J., Raghavachari, K., Rendell, A., Burant, J. C., Iyengar, S. S., Tomasi, J., Cossi, M., Rega, N., Millam, J. M., Klene, M., Knox, J. E., Cross, J. B., Bakken, V., Adamo, C., Jaramillo, J., Gomperts, R., Stratmann, R. E., Yazyev, O., Austin, A. J., Cammi, R., Pomelli, C., Ochterski, J. W., Martin, R. L., Morokuma, K., Zakrzewski, V. G., Voth, G. A., Salvador, P., Dannenberg, J. J., Dapprich, S., Daniels, A. D., Farkas, Ö., Foresman, J. B., Ortiz, J. V., Cioslowski J., and Fox, D. J. (2009) *Gaussian 09 Revision A.02*, Gaussian Inc., Wallingford, CT

The Mechanism of the Amidases: MUTATING THE GLUTAMATE ADJACENT TO THE CATALYTIC TRIAD INACTIVATES THE ENZYME DUE TO SUBSTRATE MISPOSITIONING

Brandon W. Weber, Serah W. Kimani, Arvind Varsani, Donald A. Cowan, Roger Hunter, Gerhard A. Venter, James C. Gumbart and B. Trevor Sewell

J. Biol. Chem. 2013, 288:28514-28523.
doi: 10.1074/jbc.M113.503284 originally published online August 14, 2013
